# MICROCRACK CLOSURE EFFECT ON INDENTATION TESTING OF THERMALLY SPRAYED MATERIALS

Timo Manninen[1], Reijo Kouhia[1], Erja Turunen[2], Simo-Pekka Hannula[2,3]

[1]Helsinki University of Technology, Laboratory of Structural Mechanics
P.O. Box 2100, 02015 TKK, Finland

[2]VTT
P.O. Box 1000, FIN-02044 VTT, Finland

[3]Helsinki University of Technology, Laboratory of Materials Science
P.O. Box 6200, 02015 TKK, Finland

## ABSTRACT

Depth-sensing nanoindentation is increasingly being used to study mechanical behaviour of materials. The method is also used for materials that exhibit cracks and pores. Microcracked materials, however, typically exhibit different behaviour in tension and compression due to the microcrack closure effect. The present work discusses the behaviour of microcracked heterogous materials in indentation testing. As a representative example we consider indentation testing of thermally sprayed ceramic $Al_2O_3$-coatings.

## 1 INTRODUCTION

The mechanical properties of materials are in general a function of their microstructure. Therefore establishing cross-property correlations between microstructure and properties is a central theme of materials research.

Materials prepared by thermal spraying typically have much lower Young's moduli than the corresponding bulk materials. The complex structure of thermal spray (TS) materials consist of irregular shaped lamellae formed by rapid solidification of impacting molten droplets. The structure contains large number of cracks and spherical voids. Theoretical work [1, 2, 3] explains the decisive effect of cracks on the decrease of elastic moduli. In the literature cracks are assumed to be sufficiently opened so that their behavior is similar in tension and in compression. Such an approach, however, gives acceptable approximation only at very low stresses. High compressive stresses cause microcrack closure effect, and consequently, restoration of stiffness. Recently the effect of compressive stresses on Young's moduli of thermally sprayed materials has been recognized and studied by Kroupa and his coworkers [4, 5, 6]. Motivated by theoretical and experimental results the authors conclude in [5] that "the effect of pressure, especially that of sprayed ceramics, should be taken into account in theoretical studies and in interpreting experiments in cases with high compressive stresses".

Instrumented depth-sensing indentation is increasingly being used to study mechanical behavior of thin films. Thermally sprayed ceramic coatings are brittle and relatively thin

$(150 - 300\mu\text{m})$, and therefore it is convenient to use indentation tests for measuring their elastic properties. Standard methods used to characterize the elastic properties from indentation results are based on analytical solutions to the contact problem and assume linear elastic behavior. However, a very high compressive pressure is known to exist under the tip during indentation testing [7]. It is not clear how this compressive pressure influences the results; it might induce microcrack closure effects and an increase of elastic stiffness. Evidently, the effect of pressure should be considered and taken into account in interpreting the experiments.

In the present work, the influence of microcrack closure effect in indentation testing of thermally sprayed ceramic coatings is analyzed numerically using the FE-method. The coatings produced by high velocity oxygen fuel (HVOF) thermal spray method contain microcracks and pores in diverse shapes and orientations. The nonlinear material behaviour resulting from the microcrack closure effect is modeled using a three-dimensional approach based on continuum damage mechanics.

## 2 MODELLING THE MICROCRACK CLOSURE EFFECT (MCE)

The constitutive model used for modelling the microcrack closure effect (MCE) is derived using a thermodynamic approach where the material behaviour is completely described by defining the Helmholtz free energy $\psi$ of the material. The Helmholtz free energy is a function strain $\varepsilon_{ij}$ and internal state variables.

A number of quasibrittle damage models are founded on a second order tensorial damage variable

$$D_{ij} = \sum_k d^{(k)} n_i^{(k)} n_j^{(k)} \tag{1}$$

where $d^{(k)}$ represents the density of microcracks with normal $n_i^{(k)}$. In the discrete approach [15], the damage tensor is represented by independent couples of scalar crack density values $d^{(k)}$ and corresponding orientation tensors $N_{ij}^{(k)}$.

$$D_{ij} = \sum_k d^{(k)} N_{ij}^{(k)} \tag{2}$$

The orientation tensors $N_{ij}^{(k)}$ are constructed using a fixed set of directions in the physical space. An orthonormal base is defined in $\mathbb{R}^{3\times 3}$ as follows:

$$\begin{array}{ll} N^{(1)} = e_1 \otimes e_1 & N^{(4)} = \frac{1}{2}(e_1 + e_2) \otimes (e_1 + e_2) \\ N^{(2)} = e_2 \otimes e_2 & N^{(5)} = \frac{1}{2}(e_1 + e_3) \otimes (e_1 + e_3) \\ N^{(3)} = e_3 \otimes e_3 & N^{(6)} = \frac{1}{2}(e_2 + e_3) \otimes (e_2 + e_3) \\ & N^{(7)} = \frac{1}{2}(e_1 - e_2) \otimes (e_1 - e_2) \\ & N^{(8)} = \frac{1}{2}(e_1 - e_3) \otimes (e_1 - e_3) \\ & N^{(9)} = \frac{1}{2}(e_2 - e_3) \otimes (e_2 - e_3) \end{array} \tag{3}$$

Here $(e_1, e_2, e_3)$ is a cartesian basis for $\mathbb{R}^3$. The orientation tensor base is associated with 9 crack density values $d^{(k)}$ regarded as internal state variables.

Presently it is postulated that the specific free energy can be decomposed in three parts

$$\psi = \psi_0(\varepsilon_{ij}) + \psi_1(\varepsilon_{ij}, D_{ij}) + \psi_2(\varepsilon_{ij}, D_{ij}) \tag{4}$$

The first term $\psi_0$ represents the free energy without damage. The damage effects intervene through the second term $\psi_1$. The third term $\psi_2$ contains the terms related to the microcrack

closure effect. The undamaged material is regarded as isotropic and linear elastic.

$$\rho\psi_0 = \frac{1}{2}\lambda\varepsilon_{kk}^2 + \mu\varepsilon_{ij}\varepsilon_{ij} \tag{5}$$

where $\lambda$ and $\mu$ are the Lame parameters of the undamaged material.

According to the representation theorem of tensor functions, the most general form of an isotropic scalar function depending on two symmetric second-rank tensors $\varepsilon_{ij}$ and $D_{ij}$ can be expressed as the combination of 10 basic invariants of the tensors.

$$\begin{aligned}\rho\psi \quad = \quad & \rho\psi(\varepsilon_{ii}, \varepsilon_{ij}\varepsilon_{ji}, \varepsilon_{ij}\varepsilon_{jk}\varepsilon_{ki}, D_{ii}, D_{ij}D_{ji}, D_{ij}D_{jk}D_{ki}, \varepsilon_{ij}D_{ji}, \varepsilon_{ij}\varepsilon_{jk}D_{ki}, \\ & \varepsilon_{ij}D_{jk}D_{ki}, \varepsilon_{ij}\varepsilon_{jk}D_{kl}D_{li})\end{aligned} \tag{6}$$

The material behaviour is assumed linear elastic with constant damage, and therefore the Helmholtz free energy is quadratic in $\varepsilon_{ij}$. Furthermore, since the elastic energy decreases with progressing damage, the Helmholtz free energy is assumed linear in $D_{ij}$. Eventually, a simplified representation can be used. The following simple form is used to model the damage effects [15, 16]

$$\rho\psi_1 = \alpha\varepsilon_{ij}\varepsilon_{jk}D_{ki} = \alpha\sum_a d^{(a)}\varepsilon_{ij}\varepsilon_{jk}N_{ki}^{(a)} \tag{7}$$

where $\alpha$ is an unknown material parameter.

Continuity of stress-strain response and preservation of elastic energy in closed-open sequences require , that $\psi_2$ should satisfy the conditions [14]

$$\psi_2 = 0 \quad \text{if } g = 0 \tag{8}$$

$$\frac{\partial\psi_2}{\partial\varepsilon_{pq}} = 0 \quad \text{if } g = 0 \tag{9}$$

$$\frac{\partial^2\psi_2}{\partial\varepsilon_{ab}\partial\varepsilon_{cd}} = s\frac{\partial g}{\partial\varepsilon_{ab}}\frac{\partial g}{\partial\varepsilon_{cd}} \tag{10}$$

where $s$ is a continuous scalar function and $g$ is the microcrack closure condition used.

Under uniform strain boundary conditions and dilute microcrack density, Pensee et al. [17] derived a microcrack closure condition for microcracks with orientation $N_{ij}^{(a)}$

$$g(\varepsilon_{ij}, N_{kl}^{(a)}) = M_{ij}^{(a)}\varepsilon_{ij} = 0, \tag{11}$$

where

$$M_{ij}^{(a)} = C_{ijkl}^0 N_{kl}^{(a)} = \left(\lambda\delta_{ij}\delta_{kl} + 2\mu\delta_{ik}\delta_{jl}\right)N_{kl}^{(a)} \tag{12}$$

The fourth order tensor $C_{ijkl}^0$ is the tensor of elasticity for the undamaged material. The microcrack closure condition for a particular discrete direction $N_{ij}^{(a)}$ depends only on strain and on the orientation tensor. Therefore the each discrete microcrack direction can be considered separately and the terms $d^{(k)}N_{ij}^{(k)}$ can be decoupled in the third part of the Helmholtz free energy.

The continuity conditions and the other requirements are satisfied if the third part of the Helmholtz free energy is given by

$$\rho\psi_2 = \beta\sum_a d^{(a)}H(-\varepsilon_{ij}M_{ij}^{(a)})(\varepsilon_{ij}M_{ij}^{(a)})^2, \tag{13}$$

where $\beta$ is an unknown material parameter.

The theory given above can be extended to materials for which a finite compressive stress is needed for microcrack closure. The required modification concerns only the last term, which becomes in this case

$$\rho\psi_2 = \beta \sum_a d^{(a)} H(-\varepsilon_{ij} M_{ij}^{(a)} + \gamma)(\varepsilon_{ij} M_{ij}^{(a)} - \gamma)^2, \tag{14}$$

where $\gamma$ is a material parameter describing the amount of compression needed for the microcrack closure.

In addition to the Lamé parameters of the undamaged material, the model contains three additional material parameters $\alpha$, $\beta$ and $\gamma$. The parameter $\beta$ is related to the stiffness recovery by crack closure. The stiffness recovery postulate [18] states that the stiffness in the direction normal to a closed microcrack is equal to its initial value. Imposing this recovery condition in a uniaxially microcracked state yields

$$\beta = \frac{-2\alpha}{(\lambda + 2\mu)^2} \tag{15}$$

## 3 DEPTH-SENSING INSTRUMENTED INDENTATION

Hardness tests are perhaps the most commonly used means for testing material properties. The output of a traditional hardness test is a single numeric value that describes the penetration of the indenter tip into the sample tested. Recently many technologies have moved to smaller scales. Consequently characterization of mechanical properties of materials has become more difficult. One tool that is widely used for such measurements is depth-sensing instrumented indentation, often termed "nanoindentation". It is used to determine mechanical properties of materials which are available only in a small volumes, e.g. thin films or nanocrystals. In contrast to traditional indentation, the output of an instrumented indentation test is a timeseries describing the evolution of force $P$ and displacement $h$ continuously under specified loading. The loading sequence can be specified in terms of the applied force or the indenter tip displacement and is feedback controlled by the equiplement.

Conventional analytical methods used to characterize the elastic properties from indentation load-depth curves are based on analytical solutions to the contact problem by Herz [9] and Sneddon [8]. These analytical solutions are based on following assumptions:

- The sample is isotropic, homogenous, flat, elastic half-space.
- The indenter tip is an isotropic, homogenous, elastic ball (Hertz) or a rigid revolved parabolus (Sneddon).
- Deformations are small.

The standard analysis method used the determine sample hardness $H$ or effective elastic modulus $E^*$ from measurement data is the Oliver-Pharr method.

### 3.1 THE OLIVER-PHARR METHOD

The Oliver-Pharr method is founded on Sneddon's analysis of elastic contact between a rigid axisymmetric parabolus and an elastic, isotropic, homogenous half-space. The analysis of the elastic properties is done using the unloading part of the indentation load-displacement curve. The material behaviour is supposed to be completely elastic during

**Algorithm 1** The Oliver-Pharr method.

1. Measure load $P(t)$ and displacement $h(t)$ during a loading-unloading sequence.

2. Subtract equipment frame deflection from the measured displacements.

$$h \to h - CP \tag{16}$$

   where $C$ is a compliance value determined using a reference sample.

3. Fit the powerlaw equation

$$P = c(h - h_f)^m \tag{17}$$

   where $h_f$ is the final displacement after full unloading, into the the upper 80% of the unloading part of $P(h)$. The exponent value $m = 1.5$ is used for spherical indentation.

4. Compute contact stiffness $S$

$$S := \frac{\partial P}{\partial h} = cm(h - h_f)^{m-1} \tag{18}$$

   at maximum load $P_{max}$.

5. Compute contact depth $h_c$ at maximum load using relation

$$h_c = h - \varepsilon \frac{P_{max}}{S} \tag{19}$$

   For a spherical tip the constant $\varepsilon$ equals to $\varepsilon = 0.75$.

6. Compute projected contact area $A_c = A(h_c)$ using the tip area function $A(h)$. The tip area function depends on tip geometry and is determined during equipment calibration using a reference sample.

7. Compute the elastic stifness of the sample $E_s/(1 - \nu_s^2)$ from equations

$$E^* = \sqrt{\frac{\pi}{4A_c}} S \quad \text{where} \quad \frac{1}{E^*} = \frac{1 - \nu_s^2}{E_s} + \frac{1 - \nu_i^2}{E_i} \tag{20}$$

   The effective elastic modulus $E^*$ is a function of the sample and tip elastic properties denoted by subscripts $s$ and $i$, respoctively.

8. Compute hardness $H$.

$$H := \frac{P}{A_c} \tag{21}$$

the unloading phase. The analysis of hardness and elastic properties using Oliver-Pharr method [10, 11, 12] is given below as Algorithm 1.

The Oliver-Pharr method is based on several assumptions, the most important one being that Sneddon's solution for a rigid indenter can be used with the reduced modulus of elasticity $E^*$ accounting for the elastic deformation of the tip [12]. Furthermore, the possible inelastic deformation is accounted for by subtracting the final depth $h_f$ from the total displacement in eq. (17). However, if pile-up or sinking-in happens around the indenter tip, contact depth is not equal to that estimated by eq. (19). In such a case, the effective elastic modulus is not correctly estimated by the Oliver-Pharr analysis. The results reported by Zeng et al. [13] for 11 brittle glasses and ceramic materials show, that the Oliver-Pharr method underestimates the contact depth and overestimates the effective elastic modulus for these materials.

Accurate determination of machine compliance $C$ and the tip area function $A(h)$ using a reference material sample is of great importance for the accurate characterization of the material properties. Reference samples made of synthetic amorphous silicon oxide (fused silica) are commonly used in calibration. It is worth noticing that the machine compliance value is determined by applying the Oliver-Pharr analysis to a measurement data obtained using a reference sample with known elastic properties. Therefore the compliance value also compensates errors caused by the approximations adopted in the Oliver-Pharr analysis method.

## 4 FE-SIMULATION OF MCE ON INDENTATION TESTING

Analytical solutions to Hertz contact problem are available only for isotropic, linear elastic materials. In the present work we examine the influence of the microcrack closure effect on indentation testing of materials containing large number of microcracks using numerical simulations. In order to isolate only the influence of the microcrack closure effect, the Hertzian contact damage induced during indentation testing [19] is neglected. As an example materials we consider thermally sprayed ceramic $Al_2O_3$ coatings.

### 4.1 MATERIALS

The coating samples were produced produced by the HVOF (high velocity oxygen fuel) method on an AISI 316 stainless steel substrate. The coating process is described in detail elsewhere [21]. The thickness of the coating was on the average $t_c = 0.451\,\text{mm}$ and that of the substrate was $t_s = 2.0\,\text{mm}$. The porosity of the coating was measured using image analysis method and it was approximately 5%. Figure 1 shows a micrograph of the coating cross-section.

The Young's modulus of the coating was measured using two methods: instrumented indentation technique and impulse excitation technique.

The indentation experiments were performed with Nanotest 550 nanoindentation equipment at VTT. Equipment assembly consists of a measuring unit with a pendulum structure, an optical microscope and a control unit. The calibration procedure before every experimental series included the load and depth calibration. Reference sample for the compliance determination and for depth and load calibration was fused silica ($SiO_2$). Measurements were carried out using a spherical WC-Co -tip with a radius of $R = 0.794\,\text{mm}$ under displacement control up to a maximum load of $P = 10\,\text{N}$. The indentations were made on the coating surface in the though-thickness direction. Experimental data were analysed using the standard Oliver-Pharr method. According to the indentation experiments, the Young's modulus of the coating was $E = 93.7\,\text{GPa}$.

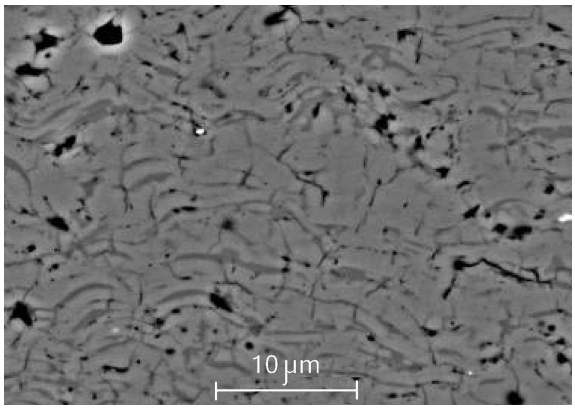


Figure 1: SEM microstructure of the coating.

The impulse excitation measurements were performed at the Laboratory of Strength of Materials in Helsinki University of Technology. In the test setup the sample is supported as a cantilever beam and its lowest natural frequency is measured before and after the coating process. Impulse hammer technique was excite small amplitude vibration in the first eigenmode. Based on the relative change of the lowest eigenfrequency, the Young's modulus of the coating is determined. The in-plane Youngs modulus was determined to be $E = (96.4 \pm 4.8)\,\mathrm{GPa}$.

### 4.2 DETERMINATION OF MATERIAL PARAMETERS

Due to rapid solidifaction and subsequent cooling of the molten droplets, the cracks formed in the coating adopt a slightly convex oval shape. A finite compressive stress $p_c$ is required to close the microcracks. The crack closing pressure dependens on the crack shape, but it is not very sensitive to crack form [4]. For typical elliptical or diamond-shaped cracks the pressure is approximately

$$\frac{p_c}{E} \approx \frac{1}{2}\frac{b}{a} \tag{22}$$

where $a$ is the radius and $b$ is the crack opening. For plasma sprayed alumina coatings the aspect ratio $\frac{b}{a}$ is typically of the order $10^{-2}...10^{-4}$ [5]. In the experiments the Youngs modulus of plasma-sprayed alumina was increasing as a function of uniaxial pressure in the whole test range from 0 to 300 MPa. No experimental data is available at the moment for HVOF alumina coatings. The HVOF coatings are, however, considerably more dense than plasma sprayed ones [22]. Therefore different values in between $\frac{a}{b} \in (0.001, 0.003)$ and the upper and lower bounds $p_c = 0$ and $p_c = -\infty$ were used in the simulations.

Apart from microcracks, thermally sprayed ceramic coatings contain also globular pores. A dilute consentration of globular randomly distributed pores lowers the elastic stiffness of the coating in an isotropic manner. The reduction of elastic properties can be approximated with [20].

$$E = E_0 \left[1 + \frac{p}{1-p}\frac{3(1-\nu_0)(9+5\nu_0)}{2(7-5\nu_0)}\right]^{-1} \tag{23}$$

$$\nu = \nu_0 \frac{E}{E_0}\left[1 + \frac{p}{1-p}\frac{3(1-\nu_0)(1+5\nu_0)}{2(7-5\nu_0)}\right] \tag{24}$$

The powder used in the spray coating process consists of $\alpha-Al_2O_3$. During the spraying metastable phases are formed and the HVOF sprayed alumina coating consists predominantly of $\gamma$-phase. The Young's modulus and Poisson ratio of this phase can be roughly estimated as $E_0 = 250\,\mathrm{GPa}$ and $\nu_0 = 0.20$. The globular pores are not taken into account in the continuum damage model. Instead, the properties of the base material are lowered accordingly. Given that the measured porosity was $p = 0.05$, the properties of the base material are $E = 225\,\mathrm{GPa}$ and $\nu = 0.185$.

The microstructure of HVOF sprayed coatings contains a variety of microcracks in different shapes and orientations. In order to express the damage in terms of microstructural parameters, the complexity of the microcracking distribution has to be reduced. Following [1] the microcrack distribution is identified as two families of strongly oblate spheroidal voids. The first family of cracks is approximately parallel to the subrate. The second family consists of random distribution of cracks perpendicular to the substrate. Consequently, the damage can be described using three crack density related state variables. Since in current case, the through-thickness direction is chosen to be along the y-axis the three crack density values are related to the nine dicrete orientations as follows:

$$d^{(2)} = d^t \tag{25}$$

$$d^{(1)} = d^{(3)} = d^{(5)} = d^{(8)} = d^p \tag{26}$$

$$d^{(4)} = d^{(6)} = d^{(7)} = d^{(9)} = d^d \tag{27}$$

The first state variable $d^t$ corresponds to density of horizontal cracking, the second variable $d^p$ descibes the density of vertical cracking and the third variable $d^d$ describes the density of inclined cracks, i.e. the amount of orientational scatter in the horizontal and vertical crack families.

In the present work, an isotropic damage orientation distribution was assumed.

$$d^t = d^p = d^d = \frac{1}{3}$$

The material parameter $\alpha$ related to the loss of elastic stiffness caused by microcracking was assigned the value

$$\alpha = 0.5739\frac{\lambda + 2\mu}{2} \tag{28}$$

This value was selected on the grounds that the reduction of elastic stiffness should correspond to the measured properties of the coating and the properties of the undamaged base material.

### 4.3 FINITE ELEMENT SIMULATION

An axisymmetric model was used for the simulation of the indentation test The model consists of a sphrical indenter tip with a radius of $R = 0.794\mathrm{mm}$ and a cylindrical sample with a radius of$R = 1.0\mathrm{mm}$ and a heigth of $H = 1.8\mathrm{mm}$. The tip comprised of 943 quadratic triangular elements (CAX6M) and the sample of 2255 elements of same type. The finite element mesh is shown in fig. 2. The tip material WC was regarded isotropic and elastic with the following properties: Young's modulus $E = 614\mathrm{GPa}$ and Poisson's ratio $\nu = 0.22$. The Coulomb coefficient of friction was $\mu = 0.085$.

In the simulations a standard indentation test was performed up to a maximum load of $P = 10\mathrm{N}$. The load was applied to the upper edge of the tip, which was constrained to remain straight. The vertical displacement and the load values were recorded for one full loading-unloading cycle.

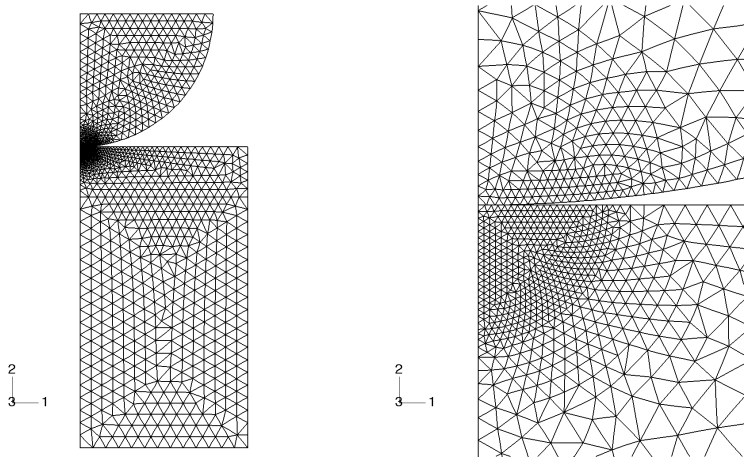


Figure 2: Finite element mesh used in numerical simulations. In the left: full model, on the right: detail.

The load-displacement curves obtained are shown in fig. fig: ph curves. The simulated data were analyzed using the Oliver-Pharr method. The compliance value was obtained by numerical simulation and analysis of indentation test on a virtual reference sample with the material properties given in [12] for fused silica glass. The results of the Oliver-Pharr analysis of the simulated $P(h)$ curves are summarized in table 1. The value $\nu = 0.185$ was used in estimating the Young's moduli from the indentation elastic stiffness values $E/(1-\nu^2)$. The given crack closure stress values are estimated based on material behavior in uniaxial compressive straining.

Table 1: The influence of material parameter $\gamma$ and the corresponding crack closure stress on indentation Young's modulus.

| $\gamma$ (MPa) | 0 | 200 | 400 | 600 | $\infty$ |
|---|---|---|---|---|---|
| $\sim p_c$ (MPa) | 0 | 125 | 250 | 375 | $\infty$ |
| $E$ (GPa) | 123 | 99 | 91 | 87 | 72 |

The results show that the indentation Young's moduli increases due to the MCE. The size of the effect is dependent on the stress which is needed for microcrack closure. This on the other hand depends on the microcrack opening, i.e. the aspect ratio of the strongly oblate, spheroidal microcracks. For a realistic aspect ratio of $\frac{a}{b} \in (0.001, 0.003)$, which correspond to $\gamma \in (200, 400)$MPa, the indentation Young's modulus equals to the experimentally measured value.

## 5 Conclusions and discussion

In the present work the influence of microcrack closure effect in indentation testing of thermally sprayed ceramic coatings is analyzed numerically using the FE-method. The nonlinear material behaviour resulting from the microcrack closure effect is modeled using a three-dimensional continuum damage mechanics -based model. The results obtained in a

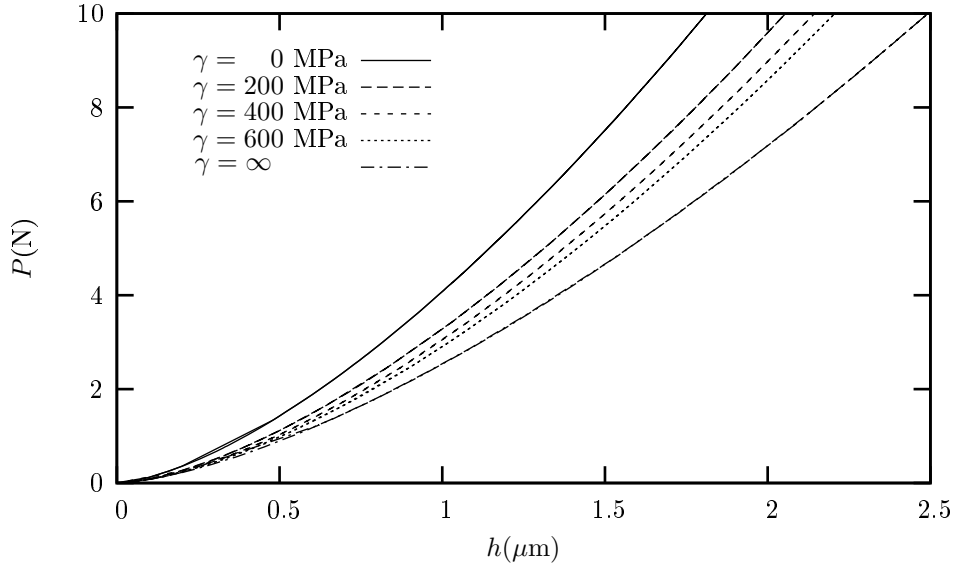


Figure 3: Simulated $P(h)$ curves for different values of parameter $\gamma$

realistic example case show that the microcrack closure effect indeed can cause a significant increase in the indentation Young's modulus. Without the microcrack closure effect, the indentation Young's modulus was $E = 72$GPa. However, with the microcrack closure effect taken into account, the indentation Young's modulus values in the range $E \in (72, 123)$GPA were obtained.

## ACKNOWLEDGEMENTS

This research has been supported by the Academy of Finland (decision number 210622).

## REFERENCES

[1] Leigh, S.-H. and Berndt, C.C. Modelling of elastic constants of plasma spray deposits with ellipsoid-shaped voids. Acta Materialia. 1999. Vol. 47, pp. 1575-1586.

[2] Sevostianov, I. and Kachanov, M. Plasma-sprayed ceramic coatings: anisotropic elastic and conductive properties in relation to the microstructure; cross-prorty correlations. Mater. Sci. Eng. 2001. Vol. A 297, pp. 235-243.

[3] Sevostianov, I., Kachanov, M., Ruud, J., Lorraine, P. and Dubois, M. Quantitative characterization of microstructures of plasma-sprayed coatings and their conductive and elastic properties. Mater. Sci. Engr. 2004. Vol. A386, pp. 164-174.

[4] Kroupa, F. and Dubsky, J. Pressure Dependence of Young's moduli of thermal sprayed materials. Scripta Materialia. 1999. Vol. 40, pp. 1249-1254.

[5] Kroupa,F. and Plesek, J. Nonlinear elastic behavior in compression of thermally sprayed materials. Mater. Sci. Engr. 2002. Vol. A328, pp. 1-7.

[6] Landa, M., Kroupa, F., Neufuss, K. and Urbanek, P. Effect of Uniaxial pressure of ultrasound velocities and elastic moduli in plasma-sprayed ceramics. J. Thermal Spray Technology. 2003. Vol. 12, pp. 226-233.

[7] Giannakopoulos A. E. & Larsson P.-L. Analysis of pyramid indentation of pressure sensitive hard metals and ceramics. Mechanics of Materials. 1997. Vol. 25, pp. 1-35.

[8] Sneddon, I. N. The relationship between load and penetration in the axisymmetric Boussineque problem for a punch of arbitrary profile. Int. J. Engr. Sci. 1965. Vol. 3, pp. 47-57. ISSN 0020-7225.

[9] Johnson, K. L. Contact Mechanics. Cambridge, UK: Cambridge University Press, 1985. ISBN: 0-521-25576-7.

[10] Oliver, W. C., and Pharr, G. M. An Improved Technique for Determining Hardness and Elastic Modulus Using Load and Displacement Sensing Indentation Experiments. Journal of Materials Research. 1992. Vol. 7, pp. 1564-1583.

[11] Vanlandingham, M. R., Review of Instrumented Indentation. Journal of Research of the National Institute of Standards and Technology. 2003. Vol. 108, pp. 249-265. ISSN 1044-677X.

[12] Knapp, J.A., Follstaedt, D.M. Myers, S.M. and Barbour, J.C. Finite-element modeling of nanoindentation. J. Applied Physics. 1999. Vol. 85, pp. 1460-1474.

[13] Zeng, K., Söderlund, E., Giannakopoulos, A. E. and Rowcliffe, D. J. Controlled indentation: A general approach to determine mechanical properties of brittle materials. Acta Materialia. 1996. Vol. 44, pp. 1127-1141. ISSN 1359-6454.

[14] Curnier, A., He, Q. and Zysset, P. Conewise linear elastic materials. J. Elasticity. 1995. Vol. 37, pp.1-38.

[15] Bargellini, R., Halm D. and Dragon, A., Modelisation de l'endommagement anisotrope par mesofissuration: vers une approche discrete. CFM 2005, 29.8-2.9.2005, Troyes, France.

[16] Challamel, N., Lanos, C. and Casandjian, C. Strain-based anisotropic damage modelling and unilateral effects. International Journal of Mechanical Sciences. 2005. Vol. 47, pp. 459-473.

[17] Pensee, V. and Kondo, D. Micromechanics of anisotropic brittle damage: comparative analysis between a stress based and a strain based formulation. Mechanics of Materials. 2003. Vol. 35, pp. 747-761.

[18] Welemane, H. and Cormery, F. An alternative 3D model for damage induced anisotropy and unilateral effect in microcracked materials. J. Phys. IV. France. 2003. Vol. 105, pp. 329-336.

[19] Licht, V., Ernst, E. and Huber, N. Simulation of the Hertzian contact damage in ceramics. Modelling Simul. Mater. Sci. Engr. 2003. Vol. 11, pp. 477-486.

[20] Kachanov, M., Tsukrov, I. and Shafiro, B. Effective moduli of solids with cavities of various shapes. Applied Mechanics Reviews. 1994. Vol. 47, pp. 151-174.

[21] Turunen, E., Varis, T., Gustafsson, T.E., Keskinen, J., Fält, T. and Hannula, S.-P. Parameter optimization of HVOF sprayed nanostructured alumina and alumina-nickel composite coatings. Surface and Coatings Technology. 2006. Vol. 200, pp. 4987-4994.

[22] Kulkarni, A., Gutleber, J., Sampath ,S., Goland, A., Lindquist, W.B., Herman, H., Allen, A.J. and Dowd, B. Studies of the microstructure and properties of dense ceramic coatings produced by high velocity oxygen-fuel combustion spraying. Materials Science and Engineering. 2004. Vol. A369, pp. 124-137.